International Journal of Developmental Neuroscience 71 (2018) 34–45

Contents lists available at ScienceDirect

International Journal of Developmental Neuroscience

journal homepage: www.elsevier.com/locate/ijdevneu

Regional volumetric abnormalities in pediatric autism revealed by structural magnetic resonance imaging

Jacob Levman[a,b,c,*], Lana Vasung[a], Patrick MacDonald[a], Sean Rowley[c], Natalie Stewart[a], Ashley Lim[a], Bryan Ewenson[c], Albert Galaburda[d], Emi Takahashi[a,b]

[a] Division of Newborn Medicine, Department of Medicine, Boston Children's Hospital, Harvard Medical School, 401 Park Dr., Boston, MA, 02215, USA
[b] Athinoula A. Martinos Center for Biomedical Imaging, Massachusetts General Hospital, Harvard Medical School, 149 13th Street, Charlestown, MA, 02129, USA
[c] Department of Mathematics, Statistics and Computer Science, St. Francis Xavier University, Antigonish, NS, B2G 2W5, Canada
[d] Department of Neurology, Beth Israel Deaconess Medical Center, Harvard Medical School, 330 Brookline Ave FD-225, Boston, MA, 02215, USA

ARTICLE INFO

Keywords:
Autistic
Development
Magnetic resonance imaging
Neuroanatomy
Volumetric

ABSTRACT

Autism is a group of complex neurodevelopmental disorders characterized by impaired social interaction, restricted and repetitive behavior. We performed a large-scale retrospective analysis of 1,996 structural magnetic resonance imaging (MRI) examinations of the brain from 1,769 autistic and neurologically typically developing patients (aged 0–32 years), and extracted regional volumetric measurements distributed across 463 brain regions of each patient. The youngest autistic patients (< 2.5 years) were diagnosed after imaging and identified retrospectively. Our study demonstrates corpus callosum volumetric abnormalities among autistic patients that are associated with brain overgrowth in early childhood (0–5 years old), followed by a shift towards known decreased volumes in later ages. Results confirm known increases in ventricular volumes among autistic populations and extends those findings to increased volumes of the choroid plexus. Our study also demonstrates distributed volumetric abnormalities among autistic patients that affect a variety of key regional white and grey matter areas of the brain potentially associated with known symptoms of autism.

1. Introduction

Autism is characterized by deficits in social reciprocity, impaired social communication and repetitive/stereotyped behaviors (Gillberg, 1993; Wing, 1997). Evidence for the existence of neuroanatomical differences between patients with autism and typically developing controls comes from a variety of neuroimaging research and post-mortem studies (Toal et al., 2005; Amaral et al., 2008). Magnetic resonance imaging (MRI) provides a wide variety of physiological/anatomical measurements of a patient's brain, information that may assist in both basic research and clinical applications. The most commonly used MRI method produces structural information related to the concentration of hydrogen protons, yielding clinically useful soft tissue contrast. In the brain, structural MRI provides for the ability to differentiate between white matter, grey matter and cerebrospinal fluid, which forms the basis for the extraction of a variety of measurements from various brain regions, such as volume measurements in the white matter, gray matter and ventricles (Fischl, 2012).

The analysis of autistic patients who have undergone structural MRI examinations has been the subject of many studies in the literature that have incorporated distributed quantification of volumetric, cortical thickness, surface area measurements etc. (Fischl, 2012). However, existing studies have been limited in the populations assessed, providing incomplete data regarding many stages of the development of autism, particularly in terms of the ages of patients included in the analysis and the number of patients included in the age range evaluated (Dziobek et al., 2010; Ecker et al., 2010, 2013, 2014; Groen et al., 2010; Haar et al., 2016; Jiao et al., 2010; Lefebvre et al., 2015; Richter et al., 2015; Schumann et al., 2010; Schaer et al., 2013, 2015; Wallace et al., 2013; Yang et al., 2016; Zielinski et al., 2014). These studies report considerably different results when trying to identify those measurements that best characterize differences between typically developing controls and autistic patients.

It is particularly challenging to assess imaging features of autism in a pediatric population, because of the structural changes that occur between childhood and maturity (Bunge et al., 2002; Casey et al., 1997; Fair et al., 2009; Gogtay et al., 2004; Reiss et al., 1996; Supekar et al., 2009; Thomas et al., 2001). Important information regarding brain function is encoded in distributed patterns of brain activity and neurological structure (Fox et al., 2005; McIntosh et al., 1996; Mesulam,

* Corresponding author at: Boston Children's Hospital, Harvard Medical School, 401 Park Dr. Boston, MA, 02215, USA.
E-mail address: jacob.levman@childrens.harvard.edu (J. Levman).

https://doi.org/10.1016/j.ijdevneu.2018.08.001
Received 3 May 2018; Received in revised form 26 July 2018; Accepted 2 August 2018
Available online 12 August 2018

1981; Vaadia et al., 1995), and identifying these patterns is particularly challenging in a pre-adult population, because of a rapidly changing anatomy and physiology, a high degree of brain plasticity, participant motion, small brain sizes and an incomplete understanding of brain development. In this paper, we hypothesize that volumetric clinical structural MRI has the potential to assist in the diagnosis of autism and to improve our understanding of brain physiology associated with the condition. This study attempts to provide a thorough assessment of the clinical potential for structural MRI by including all available autistic patients who received MRI examinations at *Boston Children's Hospital* (BCH) at 3 T producing volumetric T1 examinations compatible with the automated extraction of distributed volumetric measurements (Fischl, 2012).

2. Materials and methods

2.1. Participants

Following approval by the Institutional Review Board at BCH (informed consent was waived because of the lack of risk to patients included in this retrospective analysis), the clinical imaging electronic database at BCH was reviewed for the present analysis from 01/01/2008 until 02/24/2016, and all brain MRI examinations were included for further analysis if autistic status was noted in the patient's electronic medical records. Unfortunately, more detailed diagnostic information (such as gold standard diagnoses; e.g. Autism Diagnostic Interview-Revised [ADI-R] and Autism Diagnostic Observation Schedule [ADOS]) was not available in this dataset, an issue that is addressed in more detail in the limitations section of the discussion. Examinations deemed to be of low quality because of a large metal artifact from a patient's dental hardware, excessive patient motion, lack of a T1 structural imaging volume providing diagnostically useful axial, sagittal and coronal oriented images etc. were excluded from the study. Examinations that were inaccessible for technical reasons were also excluded. This resulted in the inclusion of 1,003 examinations from 781 autistic patients. Typically developing patients were assembled retrospectively as part of a previous study (Levman et al., 2017) by selecting participants on the basis of a normal MRI examination, as assessed by a BCH neuroradiologist, and whose medical records provided no indication of any neurological problems (patients with any known disorder were excluded such as autism, cerebral palsy, traumatic brain injury, cancer of any type, developmental delay, multiple sclerosis, tuberous sclerosis complex, stroke, neurofibromatosis, cortical dysplasia, epilepsy, attention deficit hyperactivity disorder, etc.). The same exclusion criteria applied to the autistic group was also applied to the typically developing patients. This yielded 993 examinations from 988 patients deemed neurotypical. Histograms demonstrating the age distributions for both the typically developing and autistic patients are provided in Fig. 1.

2.2. MRI data acquisition and preprocessing

All participants were imaged with clinical 3 T MRI scanners (Skyra, Siemens Medical Systems, Erlangen, Germany) at BCH yielding T1 structural volumetric images accessible through the Children's Research and Integration System (Pienaar et al., 2014). Because of the clinical and retrospective nature of this study, there is variability in the pulse sequences employed to acquire these volumetric T1 examinations, including several types of magnetization-prepared rapid gradient echo (MPRAGE) acquisitions, a few traditional T1 structural sequences as well as volumetric spoiled gradient recalled sequences. Spatial resolution varied in the x–y directions from 0.219 to 1.354 mm (mean: 0.917 mm, standard deviation: 0.124 mm). Slice thickness varied from 0.500 to 2.000 mm (mean: 0.996 mm, standard deviation: 0.197 mm). Strengths and shortcomings of the large-scale varying MR protocol approach taken in this study are addressed in the limitations section of the discussion. Automated motion correction was not performed, but examinations with substantial motion artifacts were carefully excluded based on visual assessment. T1 structural examinations were processed with FreeSurfer (Fischl, 2012). Each FreeSurfer output T1 structural examination was displayed with label map overlays and visually inspected for quality of regional segmentations. If FreeSurfer results substantially failed, they were excluded from this analysis (i.e. FreeSurfer regions-of-interest (ROIs) that do not align to the MRI and examinations where major problems were observed with an ROI such as cerebellar segmentations extending far beyond the extent of the cerebellum).

2.3. Statistical analysis

This study included the acquisition of 463 regionally distributed volumetric measurements per imaging examination, as extracted by FreeSurfer's recon-all command which processes the input examination with all available atlases (Fischl, 2012). This included all available regional volumetric measurements including whole brain measurements, whole hemisphere measurements, ventricular measurements as well as regional white and gray matter measurements in order to perform as thorough an assessment as possible. Study participants were divided into four age groups: early childhood (0–5 years old), late childhood (5–10 years old), early adolescence (10–15 years old) and late adolescence (15–20 years old). We are interested in the diagnostic potential of these clinically acquired measurements and so each FreeSurfer extracted measurement within each age range was compared in a group-wise manner (autism compared with typically developing) using receiver operating characteristic (ROC) curve analysis which is summarized with the area under the ROC curve (AUC) (Youngstrom, 2014). We also report Cohen's d statistic (positive/negative values indicate a higher/lower average value in the autistic population relative to the typically developing population). A p-value based on the standard *t*-test (Student, 1908) for two groups of samples was also computed for each comparison. This yielded a total of m = 1,852 group-wise comparisons, yielding a Bonferroni corrected threshold for achieving statistical significance of $p < 0.05/m = 2.70e^{-5}$.

In order to confirm that the findings reported are the result of group-wise differences between the autistic and typically developing patients, a statistical model was constructed based on multivariate regression, adjusting each measurement within each age range to control for group-wise differences in age, gender, estimated total intracranial volume and the leading comorbid status of the most common secondary conditions from our two groups: headaches (7% in the autistic group, 19% in the neurotypical group), ADHD (16% in the autistic group, 0% in the neurotypical group), epilepsy (13% in the autistic group, 0% in the neurotypical group), global developmental delay (26% in the autistic group, 0% in the neurotypical group), migraines (3% in the autistic group, 23% in the neurotypical group) and abdominal pain (14% in the autistic group, 11% in the neurotypical group). This model was used to adjust each volumetric measurement, in order to evaluate whether group-wise differences between our autistic and typically developing populations are the result of age, gender, intracranial volume or comorbid effects.

Our dataset includes very few exams of patients older than 20 years and so this range was not included in the group-wise age-dependent statistical analyses because of the small sample size, but was included in all scatter plots for reference. Age-dependent ROC analysis allows us to assess the diagnostic potential of any given FreeSurfer measurement and Cohen's d statistic provides useful effect size measurements at four developmental stages. Scatter plots were created to visually present measurements-of-interest from male and female patients as they vary with age, with trend lines established with a rolling average (K = 150) implemented in Matlab (Natick, MA).

A correlation analysis was also performed comparing the combined volume of each patient's ventricles (the sum of the volumes of the left

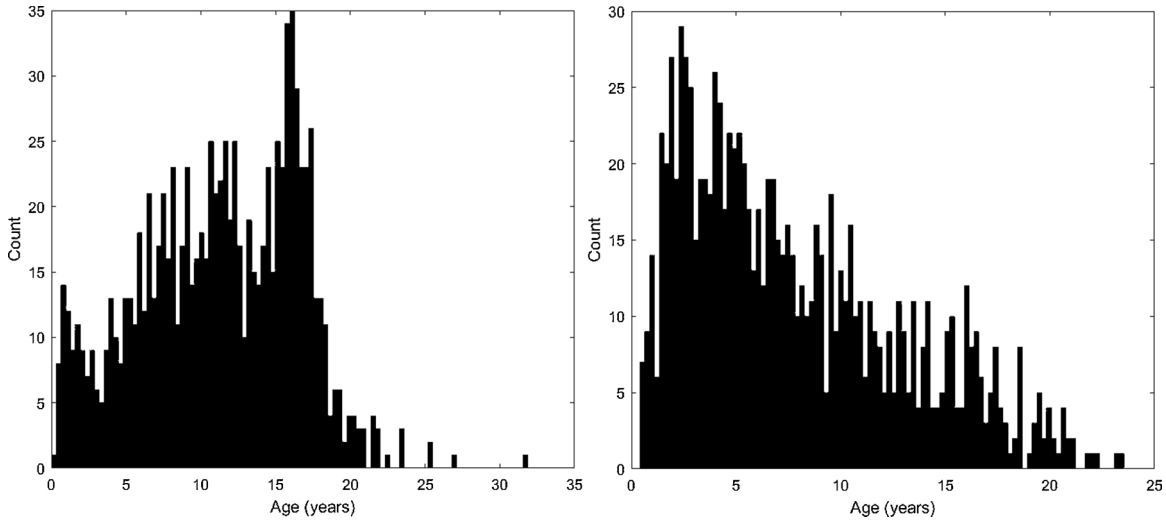

Fig. 1. Histograms demonstrating the patient population age distributions in this study's neurotypical patients (left) and autistic patients (right).

and right lateral ventricles, left and right inferior lateral ventricles, third ventricle, fourth ventricle and fifth ventricle) with the combined volume of each patient's choroid plexus (left and right volumes combined). This was performed to assess the relationship between the volume of the choroid plexus, which contributes to the production of cerebrospinal fluid (CSF) and the volume of the ventricles, which contain the CSF.

A preliminary statistical validation was performed using the independently acquired Autism Brain Imaging Data Exchange (ABIDE) dataset (Di Martino et al., 2014). The ABIDE dataset represents the results of a multi-center study with variability in data acquisition between centers. We have elected to perform a preliminary validation analysis assessing the leading seven feature measurements identified in our findings from late adolescence (see Table 1) against the single ABIDE imaging center with the most patients aged 15–20 at imaging (the USM-ABIDE data). Comparison with a single ABIDE center was selected in order to avoid having MR pulse sequence variability in the independent validation dataset. Raw (unadjusted) measurements extracted by FreeSurfer from the ABIDE dataset are directly compared with raw (unadjusted) measurements extracted by FreeSurfer from our clinical BCH dataset.

3. Results

Histograms demonstrating the age distributions for both the neurotypical and autistic groups are provided in Fig. 1. Many brain regions showed Bonferroni-corrected, statistically significant differences in volumetric measurements between patients with autism and neurotypical participants, with the leading measurements summarized in Table 1. Of the 1,852 group-wise comparisons performed, 14% exceeded the Bonferroni correction for statistical significance. Each measurement in Table 1 exceeds the Bonferroni correction in at least one age group, however, all age groupings are provided for ease of comparison. The vast majority of the leading measurements of interest identified in Table 1 have clear potential to be associated with known outward symptoms of autism.

The age-dependent, d statistic and receiver operating characteristic (ROC) curve analyses yielded several measurements that offer diagnostic potential and may help elucidate the underlying anatomical and physiological conditions associated with autism. Table 1 presents the leading measurements organized by AUC (highest AUC values are found at the top of the table), along with the associated d statistic as computed from the unadjusted measurement data extracted by FreeSurfer. Thus, the corpus callosum exhibits the largest group wise differences between autistic and neurotypical participants (ages 15–20) and substantive differences were also observed in the ventricles and regionally distributed volumetric measurements. Our multivariate-regression statistical model's adjusted data demonstrates that all reported statistically significant raw measurements remain statistically significant (Bonferroni corrected) after multivariate regression based adjustments. This was performed to confirm that the findings we are reporting are not the result of age, gender, intracranial volume, nor comorbid effects. We elected to present the raw results rather than the adjusted results for ease of comparison with future studies and because of the raw data's potential role in future diagnostic technologies.

Histograms demonstrating the age distributions for both the typically developing and autistic groups are provided in Fig. 1. The vast majority of the leading measurements of interest identified in Table 1 have clear potential to be associated with known outward symptoms of autism. Table 2 provides a collection of identified measurements of interest grouped based on their potential association with known autistic characteristics (endophenotypes), including disorders of visual and facial processing (Behrmann et al., 2006), empathy and emotional processing (Jones et al., 2010), speech and language processing (Kellerman et al., 2005; Wan and Schlaug, 2010), as well as movement and motor control (Dziuk et al., 2007). Table 2 summarizes our leading measurements-of-interest while providing bilateral effect size statistics across all age groups to help elucidate potential physiological characteristics of autism identified in this analysis. Table 3 summarizes our volumetric findings as percentages of estimated total intracranial volume (ETIV). Example scatter plots of measurements-of-interest are provided in Figs. 2–4. Note the higher variability associated with observed increased average corpus callosum volumes in the earliest years followed by volumetric reductions in later years (Fig. 2 top left), a similar inversion pattern in the volume of the white matter of the pars opercularis (Fig. 2 bottom left) and sustained increases in the volume of the third ventricle (Fig. 2 top right) and the choroid plexus (Fig. 2 bottom right). Fig. 3 presents the relationship between ventricular and choroid plexus volumes. Fig. 4 demonstrates that on average the autistic exhibit increased ETIV followed by a normalization in later years. Findings indicating increased volumes of the corpus callosum in early years occur in the context of increased whole brain volume as measured by ETIV (i.e. as a percentage of ETIV, the corpus callosum does not present differently in a young autistic population relative to the neurotypical controls). The inversion pattern observed in the corpus callosum can be seen in most of the white matter volume measurements presented (see Table 1) with the exception of the rostral anterior cingulate and the isthmus cingulate. Observed sustained increases in the

Table 1
Age-dependent ROC Analysis Results – Leading Measurements by AUC with Cohen's d statistic.

Volumetric Measurement of Interest	Measurement Type	Ages 0–5 years (AUC/d)	Ages 5–10 years (AUC/d)	Ages 10–15 years (AUC/d)	Ages 15–20 years (AUC/d)
mid posterior corpus callosum	WM Volume	(0.59/0.27)	(0.68/−0.47)	(0.74/−0.78)	(0.72/−0.66)
central corpus callosum	WM Volume	(0.57/0.22)	(0.73/−0.47)	(0.71/−0.68)	(0.69/−0.67)
posterior corpus callosum	WM Volume	(0.60/0.30)	(0.67/−0.55)	(0.67/−0.47)	(0.71/−0.68)
mid anterior corpus callosum	WM Volume	(0.61/0.32)	(0.66/−0.33)	(0.70/−0.53)	(0.65/−0.47)
third ventricle	Volume	(0.64/0.42)	(0.67/0.54)	(0.69/0.77)	(0.66/0.70)
pars opercularis	WM Volume	L (0.69/0.66) R (0.68/0.58)	L (0.55/−0.17) R (0.56/−0.19)	L (0.59/−0.25) R (0.58/−0.27)	L (0.60/−0.35) R (0.60/−0.34)
choroid plexus	Volume	L (0.61/0.39) R (0.57/0.27)	L (0.65/0.49) R (0.65/0.55)	L (0.68/0.67) R (0.69/0.74)	L (0.55/0.25) R (0.63/0.57)
cortical white matter (each hemisphere)	WM Volume	L (0.69/0.65) R (0.68/0.60)	L (0.57/−0.20) R (0.56/−0.18)	L (0.58/−0.30) R (0.57/−0.25)	L (0.56/−0.22) R (0.56/−0.20)
cortical white matter (combined hemispheres)	WM Volume	(0.68/0.63)	(0.57/−0.19)	(0.57/−0.28)	(0.56/−0.21)
rostral middle frontal	WM Volume	L (0.68/0.62) R (0.68/0.60)	L (0.56/−0.17) R (0.59/−0.25)	L (0.55/−0.20) R (0.52/−0.09)	L (0.50/−0.03) R (0.52/−0.09)
lateral ventricle	Volume	L (0.66/0.46) R (0.68/0.48)	L (0.67/0.50) R (0.67/0.55)	L (0.68/0.71) R (0.65/0.65)	L (0.60/0.50) R (0.63/0.56)
inferior temporal	WM Volume	L (0.68/0.62) R (0.68/0.60)	L (0.56/−0.06) R (0.54/−0.11)	L (0.60/−0.32) R (0.54/−0.13)	L (0.60/−0.31) R (0.55/−0.18)
Caudate	GM Volume	L (0.66/0.53) R (0.68/0.62)	L (0.52/0.06) R (0.51/0.01)	L (0.57/0.23) R (0.60/0.35)	L (0.52/−0.13) R (0.53/−0.14)
superior temporal	WM Volume	L (0.67/0.61) R (0.64/0.52)	L (0.52/−0.10) R (0.56/−0.15)	L (0.53/−0.09) R (0.56/−0.19)	L (0.53/−0.14) R (0.59/−0.28)
Precentral	WM Volume	L (0.67/0.61) R (0.66/0.57)	L (0.55/−0.17) R (0.54/−0.10)	L (0.55/−0.17) R (0.55/−0.18)	L (0.53/−0.14) R (0.53/−0.12)
Precuneus	WM Volume	L (0.67/0.61) R (0.65/0.52)	L (0.54/−0.12) R (0.54/−0.08)	L (0.53/−0.13) R (0.53/−0.09)	L (0.52/−0.03) R (0.54/0.12)
Fusiform	WM Volume	L (0.67/0.59) R (0.67/0.58)	L (0.58/−0.25) R (0.58/−0.28)	L (0.63/−0.38) R (0.58/−0.23)	L (0.61/−0.38) R (0.58/−0.26)
fourth ventricle	Volume	(0.67/0.52)	(0.51/0.13)	(0.54/0.32)	(0.48/0.02)
lateral orbitofrontal	WM Volume	L (0.67/0.62) R (0.66/0.56)	L (0.58/−0.28) R (0.58/−0.28)	L (0.55/−0.20) R (0.55/−0.24)	L (0.55/−0.16) R (0.54/−0.14)
estimated total intracranial volume	Volume	(0.67/0.55)	(0.52/−0.04)	(0.50/−0.05)	(0.50/−0.09)
Supramarginal	WM Volume	L (0.67/0.60) R (0.65/0.48)	L (0.52/−0.03) R (0.50/0.03)	L (0.53/−0.05) R (0.56/−0.12)	L (0.55/−0.14) R (0.54/−0.14)
superior frontal	WM Volume	L (0.64/0.52) R (0.67/0.57)	L (0.57/−0.18) R (0.56/−0.19)	L (0.53/−0.13) R (0.54/−0.10)	L (0.52/0.04) R (0.52/−0.04)
middle temporal	WM Volume	L (0.67/0.56) R (0.67/0.59)	L (0.56/−0.11) R (0.55/−0.16)	L (0.54/−0.18) R (0.53/−0.03)	L (0.56/−0.08) R (0.57/−0.27)
inferior temporal gyrus	GM Volume	L (0.65/0.56) R (0.67/0.59)	L (0.53/−0.09) R (0.49/0.00)	L (0.51/−0.05) R (0.54/0.16)	L (0.50/0.02) R (0.56/0.17)
caudal anterior cingulate	WM Volume	L (0.65/0.54) R (0.67/0.54)	L (0.53/−0.08) R (0.56/−0.11)	L (0.58/−0.27) R (0.56/−0.18)	L (0.60/−0.36) R (0.56/−0.27)
rostral anterior cingulate	WM Volume	L (0.64/0.47) R (0.67/0.56)	L (0.55/−0.19) R (0.49/0.01)	L (0.51/0.02) R (0.54/0.10)	L (0.54/0.09) R (0.56/0.21)
inferior part of the precentral sulcus	GM Volume	L (0.67/0.58) R (0.61/0.42)	L (0.52/−0.08) R (0.52/−0.10)	L (0.51/−0.11) R (0.51/0.12)	L (0.51/−0.03) R (0.54/−0.08)
inferior temporal cortex	GM Volume	L (0.66/0.59) R (0.66/0.56)	L (0.53/−0.10) R (0.52/−0.05)	L (0.53/−0.10) R (0.55/0.15)	L (0.50/0.02) R (0.55/0.12)
lateral occipital	WM Volume	L (0.66/0.57) R (0.62/0.43)	L (0.58/−0.18) R (0.53/−0.09)	L (0.58/−0.33) R (0.58/−0.29)	L (0.55/−0.07) R (0.55/−0.13)
short insular gyrus	GM Volume	L (0.66/0.59) R (0.64/0.51)	L (0.49/−0.05) R (0.52/−0.07)	L (0.55/0.17) R (0.56/0.16)	L (0.53/−0.13) R (0.53/−0.10)
Lingual	WM Volume	L (0.66/0.56) R (0.64/0.49)	L (0.62/−0.38) R (0.58/−0.20)	L (0.63/−0.39) R (0.62/−0.34)	L (0.59/−0.30) R (0.56/−0.21)
planum polare	GM Volume	L (0.66/0.57) R (0.61/0.40)	L (0.56/−0.18) R (0.53/−0.07)	L (0.53/−0.08) R (0.50/0.01)	L (0.57/−0.22) R (0.53/−0.11)
Precuneus cortex	GM Volume	L (0.61/0.45) R (0.58/0.34)	L (0.50/0.01) R (0.51/0.07)	L (0.57/0.19) R (0.59/0.30)	L (0.59/0.34) R (0.66/0.50)
isthmus cingulate	WM Volume	L (0.66/0.48) R (0.64/0.47)	L (0.50/0.02) R (0.50/0.02)	L (0.53/0.13) R (0.50/0.00)	L (0.50/0.05) R (0.56/−0.22)
Insula	WM Volume	L (0.65/0.57) R (0.66/0.56)	L (0.54/−0.23) R (0.55/−0.22)	L (0.52/−0.15) R (0.52/−0.14)	L (0.52/0.02) R (0.53/−0.14)
superior temporal cortex	GM Volume	L (0.66/0.61) R (0.62/0.43)	L (0.52/−0.12) R (0.55/−0.17)	L (0.53/0.06) R (0.51/0.01)	L (0.56/0.16) R (0.52/0.06)
gyrus rectus	GM Volume	L (0.50/0.09) R (0.51/0.21)	L (0.55/0.14) R (0.50/0.01)	L (0.66/0.55) R (0.57/0.23)	L (0.60/0.34) R (0.56/0.18)
rostral middle frontal cortex	GM Volume	L (0.66/0.56) R (0.63/0.49)	L (0.53/−0.11) R (0.55/−0.14)	L (0.50/0.01) R (0.56/0.19)	L (0.55/0.18) R (0.54/0.18)
inferior parietal	WM Volume	L (0.66/0.56) R (0.60/0.30)	L (0.48/0.01) R (0.48/0.02)	L (0.54/−0.14) R (0.52/−0.05)	L (0.51/−0.06) R (0.53/−0.08)
caudal middle frontal	WM Volume	L (0.66/0.57) R (0.63/0.44)	L (0.54/−0.14) R (0.55/−0.17)	L (0.57/−0.28) R (0.55/−0.17)	L (0.56/−0.23) R (0.57/−0.20)
superior parietal	WM Volume	L (0.66/0.53) R (0.60/0.35)	L (0.58/−0.25) R (0.57/−0.22)	L (0.54/−0.15) R (0.53/−0.11)	L (0.58/−0.24) R (0.52/−0.13)

Abbreviations/Symbols: R = right; L = Left; GM = gray matter; WM = white matter; AUC = area under the ROC curve; d = Cohen's d statistic.

Table 2
Summary of Measurements with Effect Sizes Potentially Associated with Known Autistic Characteristics.

Autistic Characteristics	Potentially Associated Measurements	Brain Regions Affected	Ages 0–5 L&R: d	Ages 5–10 L&R: d	Ages 10–15 L&R: d	Ages 15–20 L&R: d
Facial & Visual Processing	Precuneus WM	Parietal	L (d = 0.61) R (d = 0.52)	L (d = −0.12) R (d = −0.08)	L (d = −0.13) R (d = −0.09)	L (d = −0.03) R (d = 0.12)
	Precuneus GM	Parietal	L (d = 0.45) R (d = 0.34)	L (d = 0.01) R (d = 0.07)	L (d = 0.19) R (d = 0.30)	L (d = 0.34) R (d = 0.50)
	Inferior parietal WM	Parietal	L (d = 0.56) R (d = 0.30)	L (d = 0.01) R (d = 0.02)	L (d = −0.14) R (d = −0.05)	L (d = −0.06) R (d = −0.08)
	Inferior temporal WM	Temporal	L (d = 0.62) R (d = 0.60)	L (d = −0.06) R (d = −0.11)	L (d = −0.32) R (d = −0.13)	L (d = −0.31) R (d = −0.18)
	Superior temporal WM	Temporal	L (d = 0.61) R (d = 0.52)	L (d = −0.10) R (d = −0.15)	L (d = −0.09) R (d = −0.19)	L (d = −0.14) R (d = −0.28)
	Superior temporal GM	Temporal	L (d = 0.61) R (d = 0.43)	L (d = −0.12) R (d = −0.17)	L (d = 0.06) R (d = 0.01)	L (d = 0.16) R (d = 0.06)
	Fusiform WM	Temporal	L (d = 0.59) R (d = 0.58)	L (d = −0.25) R (d = −0.28)	L (d = −0.38) R (d = −0.23)	L (d = −0.38) R (d = −0.26)
	Inferior temporal gyrus GM	Temporal	L (d = 0.56) R (d = 0.59)	L (d = −0.09) R (d = 0.00)	L (d = −0.05) R (d = 0.16)	L (d = 0.02) R (d = 0.17)
	Lingual WM	Occipital	L (d = 0.56) R (d = 0.49)	L (d = −0.38) R (d = −0.20)	L (d = −0.39) R (d = −0.34)	L (d = −0.30) R (d = −0.21)
Speech & Language Processing	Pars opercularis WM	Frontal	L (d = 0.66) R (d = 0.58)	L (d = −0.17) R (d = −0.19)	L (d = −0.25) R (d = −0.27)	L (d = −0.35) R (d = −0.34)
	Supramarginal WM	Parietal	L (d = 0.60) R (d = 0.48)	L (d = −0.03) R (d = 0.03)	L (d = −0.05) R (d = −0.12)	L (d = −0.14) R (d = −0.14)
	Superior temporal WM	Temporal	L (d = 0.61) R (d = 0.52)	L (d = −0.10) R (d = −0.15)	L (d = −0.09) R (d = −0.19)	L (d = −0.14) R (d = −0.28)
	Superior temporal GM	Temporal	L (d = 0.61) R (d = 0.43)	L (d = −0.12) R (d = −0.17)	L (d = 0.06) R (d = 0.01)	L (d = 0.16) R (d = 0.06)
	Planum polare GM	Temporal	L (d = 0.57) R (d = 0.40)	L (d = −0.18) R (d = −0.07)	L (d = −0.08) R (d = 0.01)	L (d = −0.22) R (d = −0.11)
	Fusiform WM	Temporal	L (d = 0.59) R (d = 0.58)	L (d = −0.25) R (d = −0.28)	L (d = −0.38) R (d = −0.23)	L (d = −0.38) R (d = −0.26)
	Middle temporal WM	Temporal	L (d = 0.56) R (d = 0.59)	L (d = −0.11) R (d = −0.16)	L (d = −0.18) R (d = −0.03)	L (d = −0.08) R (d = −0.27)
	Lingual WM	Occipital	L (d = 0.56) R (d = 0.49)	L (d = −0.38) R (d = −0.20)	L (d = −0.39) R (d = −0.34)	L (d = −0.30) R (d = −0.21)
	Caudate		L (d = 0.53) R (d = 0.62)	L (d = 0.06) R (d = 0.01)	L (d = 0.23) R (d = 0.35)	L (d = −0.13) R (d = −0.14)
Movement and Motor Control	Precentral WM	Frontal	L (d = 0.61) R (d = 0.57)	L (d = −0.17) R (d = −0.10)	L (d = −0.17) R (d = −0.18)	L (d = −0.14) R (d = −0.12)
	Inferior part of the precentral sulcus GM	Frontal	L (d = 0.58) R (d = 0.42)	L (d = −0.08) R (d = −0.10)	L (d = −0.11) R (d = 0.12)	L (d = −0.03) R (d = −0.08)
	Precuneus WM	Parietal	L (d = 0.61) R (d = 0.52)	L (d = −0.12) R (d = −0.08)	L (d = −0.13) R (d = −0.09)	L (d = −0.03) R (d = 0.12)
	Precuneus GM	Parietal	L (d = 0.45) R (d = 0.34)	L (d = 0.01) R (d = 0.07)	L (d = 0.19) R (d = 0.30)	L (d = 0.34) R (d = 0.50)
	Supramarginal WM	Parietal	L (d = 0.60) R (d = 0.48)	L (d = −0.03) R (d = 0.03)	L (d = −0.05) R (d = −0.12)	L (d = −0.14) R (d = −0.14)
	Superior parietal WM	Parietal	L (d = 0.53) R (d = 0.35)	L (d = −0.25) R (d = −0.22)	L (d = −0.15) R (d = −0.11)	L (d = −0.24) R (d = −0.13)
	Superior temporal WM	Temporal	L (d = 0.61) R (d = 0.52)	L (d = −0.10) R (d = −0.15)	L (d = −0.09) R (d = −0.19)	L (d = −0.14) R (d = −0.28)
	Superior temporal GM	Temporal	L (d = 0.61) R (d = 0.43)	L (d = −0.12) R (d = −0.17)	L (d = 0.06) R (d = 0.01)	L (d = 0.16) R (d = 0.06)
	Inferior temporal gyrus GM	Temporal	L (d = 0.56) R (d = 0.59)	L (d = −0.09) R (d = 0.00)	L (d = −0.05) R (d = 0.16)	L (d = 0.02) R (d = 0.17)
	Lateral occipital WM	Occipital	L (d = 0.57) R (d = 0.43)	L (d = −0.18) R (d = −0.09)	L (d = −0.33) R (d = −0.29)	L (d = −0.07) R (d = −0.13)
	Caudate		L (d = 0.53) R (d = 0.62)	L (d = 0.06) R (d = 0.01)	L (d = 0.23) R (d = 0.35)	L (d = −0.13) R (d = −0.14)
Empathy Deficits & Emotional Processing	Lateral orbitofrontal WM	Frontal	L (d = 0.62) R (d = 0.56)	L (d = −0.28) R (d = −0.28)	L (d = −0.20) R (d = −0.24)	L (d = −0.16) R (d = −0.14)
	Superior frontal WM	Frontal	L (d = 0.52) R (d = 0.57)	L (d = −0.18) R (d = −0.19)	L (d = −0.13) R (d = −0.10)	L (d = 0.04) R (d = −0.04)
	Caudal anterior cingulate WM	Frontal	L (d = 0.54) R (d = 0.54)	L (d = −0.08) R (d = −0.11)	L (d = −0.27) R (d = −0.18)	L (d = −0.36) R (d = −0.27)
	Rostral anterior cingulate WM	Frontal	L (d = 0.47) R (d = 0.56)	L (d = −0.19) R (d = 0.01)	L (d = 0.02) R (d = 0.10)	L (d = 0.09) R (d = 0.21)
	Precuneus WM	Parietal	L (d = 0.61) R (d = 0.52)	L (d = −0.12) R (d = −0.08)	L (d = −0.13) R (d = −0.09)	L (d = −0.03) R (d = 0.12)
	Precuneus GM	Parietal	L (d = 0.45) R (d = 0.34)	L (d = 0.01) R (d = 0.07)	L (d = 0.19) R (d = 0.30)	L (d = 0.34) R (d = 0.50)
	Supramarginal WM	Parietal	L (d = 0.60) R (d = 0.48)	L (d = −0.03) R (d = 0.03)	L (d = −0.05) R (d = −0.12)	L (d = −0.14) R (d = −0.14)
	Inferior parietal WM	Parietal	L (d = 0.56) R (d = 0.30)	L (d = 0.01) R (d = 0.02)	L (d = −0.14) R (d = −0.05)	L (d = −0.06) R (d = −0.08)
	Superior temporal WM	Temporal	L (d = 0.61) R (d = 0.52)	L (d = −0.10) R (d = −0.15)	L (d = −0.09) R (d = −0.19)	L (d = −0.14) R (d = −0.28)
	Superior temporal GM	Temporal	L (d = 0.61) R (d = 0.43)	L (d = −0.12) R (d = −0.17)	L (d = 0.06) R (d = 0.01)	L (d = 0.16) R (d = 0.06)
	Insula WM		L (d = 0.57) R (d = 0.56)	L (d = −0.23) R (d = −0.22)	L (d = −0.15) R (d = −0.14)	L (d = 0.02) R (d = −0.14)
	Short insular gyrus GM		L (d = 0.59) R (d = 0.51)	L (d = −0.05) R (d = −0.07)	L (d = 0.17) R (d = 0.16)	L (d = −0.13) R (d = −0.10)
	Caudate		L (d = 0.53) R (d = 0.62)	L (d = 0.06) R (d = 0.01)	L (d = 0.23) R (d = 0.35)	L (d = −0.13) R (d = −0.14)

Abbreviations/Symbols: R = right; L = Left; GM = gray matter; WM = white matter; d = Cohen's d statistic.

Table 3
Age-dependent ROC Analysis Results – Leading Volumetric Measurements as a Percentage of ETIV, AUC (Cohen's d).

Volumetric Measurement of Interest	Measurement Type	Ages 0–5 years AUC (d)	Ages 5–10 years AUC (d)	Ages 10–15 years AUC (d)	Ages 15–20 years AUC (d)
Mid posterior corpus callosum	WM Volume	0.51 (0.07)	0.68 (−0.42)	0.76 (−0.78)	0.72 (−0.55)
Hypointensities	WM Volume	0.63 (−0.30)	0.53 (0.30)	0.58 (0.35)	0.74 (0.88)
Central corpus callosum	WM Volume	0.48 (0.00)	0.72 (−0.42)	0.70 (−0.65)	0.69 (−0.65)
3rd Ventricle Volume	Volume	0.54 (0.22)	0.68 (0.61)	0.72 (0.85)	0.71 (0.77)
Posterior corpus callosum	WM Volume	0.51 (−0.03)	0.66 (−0.53)	0.68 (−0.49)	0.72 (−0.62)
Choroid plexus	Volume	L 0.49 (0.00), R 0.53 (−0.08)	L 0.67 (0.55), R 0.67 (0.61)	L 0.70 (0.73), R 0.70 (0.78)	L 0.58 (0.35), R 0.64 (0.66)
Mid anterior corpus callosum	WM Volume	0.53 (0.17)	0.66 (−0.32)	0.70 (−0.51)	0.64 (−0.47)
Lateral ventricle	Volume	L 0.60 (0.38), R 0.62 (0.41)	L 0.69 (0.56), R 0.68 (0.60)	L 0.70 (0.76), R 0.67 (0.69)	L 0.61 (0.56), R 0.64 (0.62)
Unsegmented white matter	WM Volume	L 0.62 (0.32), R 0.62 (0.32)	L 0.60 (−0.31), R 0.61 (−0.34)	L 0.68 (−0.60), R 0.66 (−0.55)	L 0.69 (−0.60), R 0.67 (−0.52)
Precuneus	GM Volume	L 0.50 (0.04), R 0.56 (−0.12)	L 0.51 (0.06), R 0.54 (0.15)	L 0.56 (0.26), R 0.59 (0.41)	L 0.62 (0.49), R 0.68 (0.70)
Cerebellum	GM Volume	L 0.68 (−0.55) R 0.67 (−0.50)	L 0.58 (−0.25), R 0.56 (−0.17)	L 0.57 (−0.27), R 0.57 (−0.25)	L 0.57 (−0.27), R 0.57 (−0.11)
Pericalcarine	WM Volume	L 0.56 (0.19), R 0.52 (0.03)	L 0.63 (−0.42), R 0.57 (−0.24)	L 0.66 (−0.54), R 0.65 (−0.44)	L 0.59 (−0.20), R 0.55 (−0.17)
Inferior lateral ventricle	Volume	L 0.57 (0.27), R 0.53 (0.20)	L 0.62 (0.45), R 0.59 (0.39)	L 0.66 (0.61), R 0.63 (0.54)	L 0.59 (0.54), R 0.63 (0.43)
Lingual	WM Volume	L 0.58 (0.25), R 0.55 (0.18)	L 0.63 (-0.44), R 0.58 (-0.22)	L 0.66 (-0.46), R 0.64 (-0.38)	L 0.60 (0.33), R 0.57 (-0.24)
Suborbital sulcus	GM Volume	L 0.55 (−0.06), R 0.54 (0.14)	L 0.51 (0.02), R 0.50 (0.02)	L 0.58 (0.24), R 0.59 (0.32)	L 0.65 (0.60), R 0.55 (0.16)
Pars opercularis	WM Volume	L 0.65 (0.47), R 0.61 (0.37)	L 0.56 (−0.22), R 0.57 (−0.23)	L 0.61 (−0.31), R 0.59 (−0.32)	L 0.62 (−0.42), R 0.61 (−0.37)
Cortical white matter volume	WM Volume	L 0.62 (0.40), R 0.58 (0.27)	L 0.60 (-0.34), R 0.58 (-0.29)	L 0.65 (-0.48), R 0.62 (-0.39)	L 0.61 (-0.31), R 0.60 (-0.28)
Paracentral	GM Volume	L 0.55 (−0.15), R 0.56 (−0.16)	L 0.51 (0.01), R 0.51 (0.02)	L 0.55 (0.16), R 0.55 (0.16)	L 0.65 (0.56), R 0.65 (0.56)
Medial orbitofrontal	GM Volume	L 0.58 (−0.07), R 0.46 (0.04)	L 0.55 (0.15), R 0.53 (0.12)	L 0.60 (0.42), R 0.59 (0.34)	L 0.65 (0.57), R 0.61 (0.43)
Non WM hypointensities	Volume	0.47 (−0.04)	0.58 (0.09)	0.65 (0.25)	0.63 (0.18)
Superior frontal gyrus	GM Volume	L 0.57 (−0.14), R 0.55 (−0.12)	L 0.51 (−0.09), R 0.51 (−0.01)	L 0.58 (0.29), R 0.62 (0.39)	L 0.65 (0.53), R 0.64 (0.49)
Gyrus rectus	GM Volume	L 0.61 (−0.24), R 0.57 (−0.13)	L 0.55 (0.22), R 0.53 (0.12)	L 0.65 (0.63), R 0.56 (0.30)	L 0.61 (0.48), R 0.57 (0.29)
Cerebellum	WM Volume	L 0.50 (0.00), R 0.51 (0.11)	L 0.58 (−0.15), R 0.63 (−0.29)	L 0.63 (−0.28), R 0.65 (−0.41)	L 0.48 (0.21), R 0.47 (0.18)
Thalamus	GM Volume	L 0.58 (−0.28), R 0.62 (−0.34)	L 0.59 (−0.28), R 0.55 (−0.17)	L 0.65 (−0.39), R 0.55 (−0.11)	L 0.48 (0.11), R 0.49 (0.06)
Marginal branch of the cingulate sulcus	GM Volume	L 0.53 (−0.04), R 0.52 (−0.06)	L 0.50 (0.01), R 0.49 (0.01)	L 0.56 (0.19), R 0.55 (0.13)	L 0.64 (0.56), R 0.62 (0.52)
Paracentral gyrus and sulcus	GM Volume	L 0.59 (−0.27), R 0.61 (−0.39)	L 0.54 (0.01), R 0.55 (0.13)	L 0.56 (0.13), R 0.59 (0.24)	L 0.63 (0.49), R 0.64 (0.47)
Brodmann's area 3b	GM Volume	L 0.55 (−0.26), R 0.55 (−0.10)	L 0.54 (0.13), R 0.52 (0.05)	L 60 (0.32), R 0.54 (0.10)	L 0.61 (0.51), R 0.64 (0.47)
Fusiform	WM Volume	L 0.61 (0.35), R 0.59 (0.34)	L 0.60 (−0.34), R 0.60 (−0.37)	L 0.64 (−0.51), R 0.59 (−0.31)	L 0.63 (−0.49), R 0.61 (−0.37)
Total cortical white matter volume	WM Volume	0.60 (0.34)	0.60 (−0.32)	0.64 (−0.44)	0.61 (−0.30)
Brodmann's area 3a	GM Volume	L 0.62 (−0.36), R 0.58 (−0.23)	L 0.54 (0.09), R 0.54 (0.05)	L 0.60 (0.36), R 0.56 (0.22)	L 0.63 (0.44), R 0.64 (0.48)
Postcentral	GM Volume	L 0.57 (−0.24), R 0.58 (−0.22)	L 0.51 (−0.01), R 0.50 (0.08)	L 0.59 (0.31), R 0.54 (0.16)	L 0.60 (0.41), R 0.64 (0.43)
Lateral orbitofrontal	WM Volume	L 0.60 (0.41), R 0.58 (0.28)	L 0.64 (−0.43), R 0.63 (−0.39)	L 0.57 (−0.28), R 0.59 (−0.32)	L 0.55 (−0.14), R 0.53 (−0.13)

Abbreviations/Symbols: R = right; L = Left; GM = gray matter; WM = white matter; AUC = area under the ROC curve; d = Cohen's d statistic; ETIV Estimated Total Intracranial Volume.

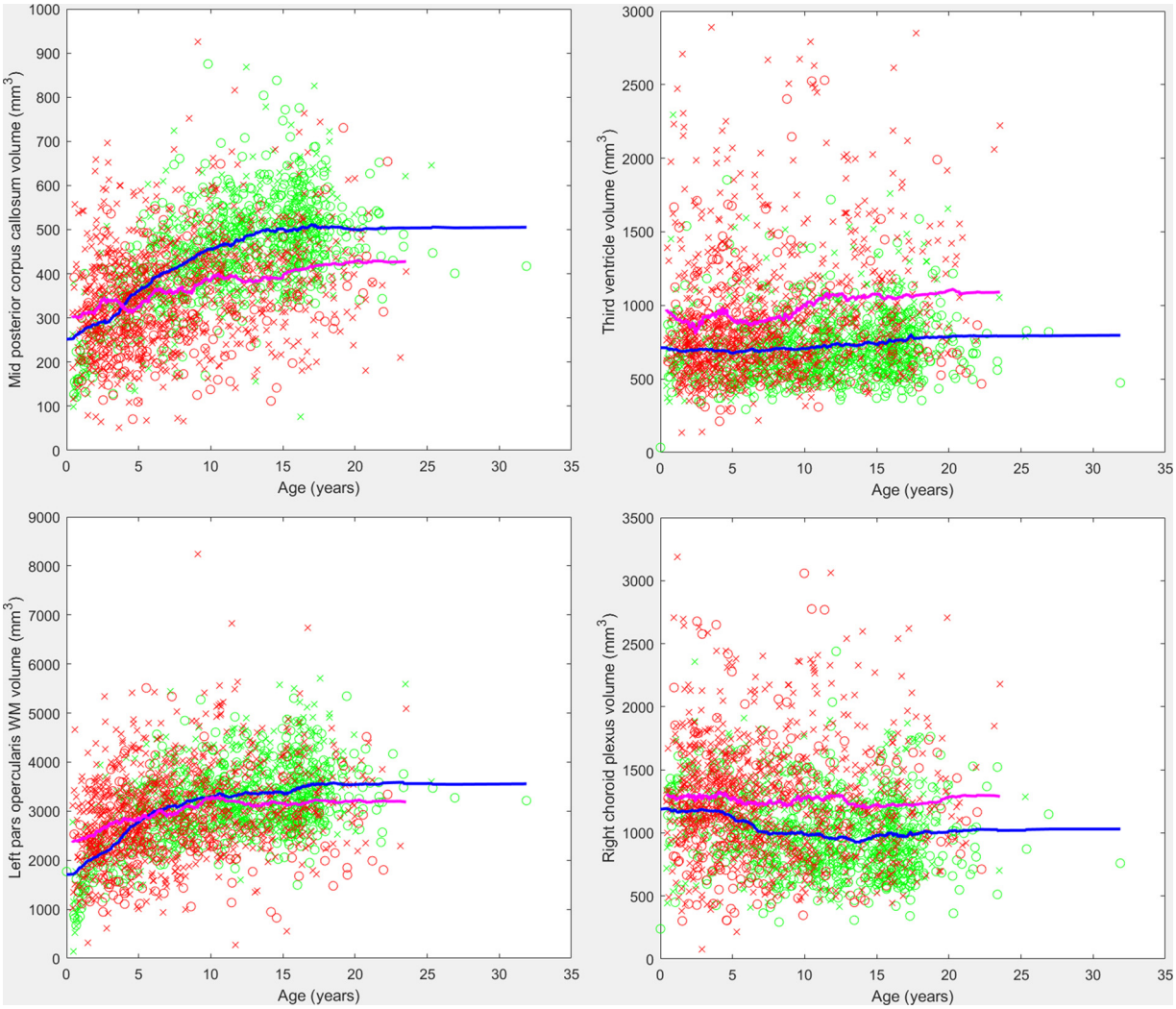

Fig. 2. Scatter plots of the volumes of four regions of interest, including the mid posterior corpus callosum (upper left), the third ventricle (upper right), the left pars opercularis white matter (lower left) and the right choroid plexus (lower right). Scatter plots present patients with autism (red) and neurotypical participants (green). Male patients are represented with an 'x', females with an 'o'. Trend lines are plotted (magenta = autistic, blue = neurotypical). (For interpretation of the references to colour in this figure legend, the reader is referred to the web version of this article.)

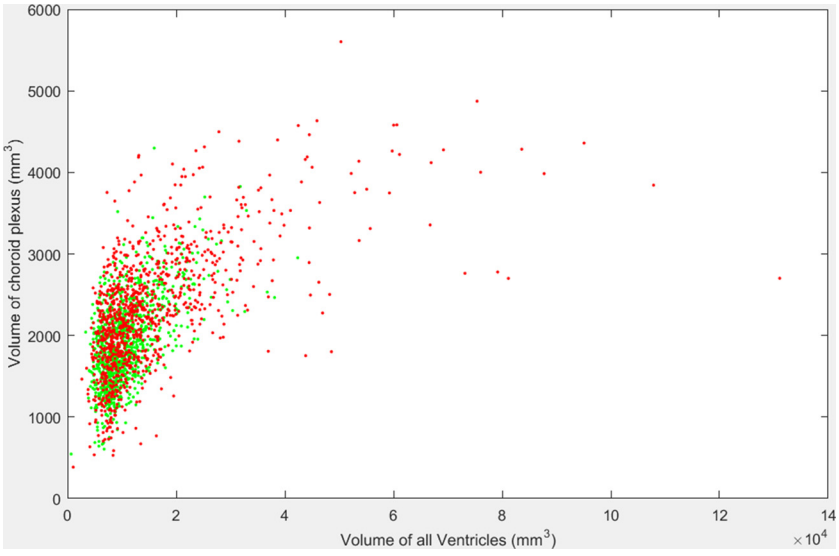

Fig. 3. Scatter plot of each patient's combined choroid plexus volume (sum of the left and right volumes) as it varies with the sum of the patient's ventricular volumes. Patients with autism are presented in red, neurotypical patients are presented in green. (For interpretation of the references to colour in this figure legend, the reader is referred to the web version of this article.)

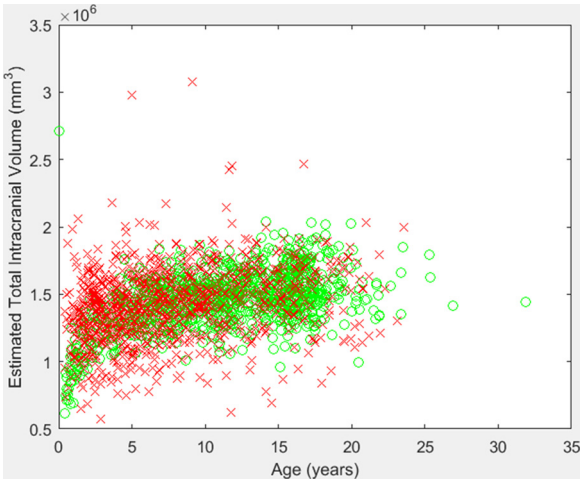

Fig. 4. Scatter plot of each patient's estimated total intracranial volume as it varies with age. Patients with autism are presented in red, neurotypical patients are presented in green. (For interpretation of the references to colour in this figure legend, the reader is referred to the web version of this article.)

third ventricle volume extend to all of the other ventricles and to both the left and right choroid plexus volumes. The gray matter regions exhibiting the most group-wise differences tended to exhibit elevated volumes in the earliest years followed by a period of normalization with the exception of the precuneus and the gyrus rectus. We also performed a correlation analysis comparing the combined volume of each patient's ventricles (the sum of the volumes of the left and right lateral ventricles, left and right inferior lateral ventricles, third ventricle, fourth ventricle and fifth ventricle) with the combined volume of each patient's choroid plexus (left and right volumes combined). Results demonstrate a positive correlation between the choroid plexus volume and ventricular volumes (correlation 0.60, $p = 5.9e^{-195}$), with autistic patients who exhibit elevated ventricular volumes also tending to exhibit elevated choroid plexus volumes (see Fig. 3). In order to support a thorough analysis, all available brain atlases from FreeSurfer were included in this study, resulting in Tables 1–3 reporting overlapping regions of interest including measurements across a region's cortex as well as localized gyral, sulcal and lobular measurements when available.

We have performed a preliminary validation with the Autism Brain Imaging Data Exchange (ABIDE) public dataset (Di Martino et al., 2014). Results confirm these leading volumetric measurements relative to our BCH data: posterior corpus callosum (BCH: $d = -0.66$, ABIDE: $d = -0.52$), central corpus callosum (BCH: $d = -0.67$, ABIDE: AUC $= -0.39$), mid posterior corpus callosum (BCH: $d = -0.66$, ABIDE: $d = -0.26$), mid anterior corpus callosum (BCH: $d = -0.47$, ABIDE: $d = -0.59$), third ventricle (BCH: $d = 0.70$, ABIDE: $d = 0.48$), the right choroid plexus (BCH: $d = 0.57$, ABIDE: $d = 0.39$), and the right lateral ventricle (BCH: $d = 0.56$, ABIDE: $d = 0.35$). This confirmed our findings in each of our leading measurements (late adolescence) exhibiting reduced separation between the neurotypical and autistic groups in the ABIDE dataset, with the exception of the mid anterior corpus callosum which exhibits a larger effect size in ABIDE.

4. Discussion

We performed a large-scale volumetric analysis of structural MRI examinations of the brain in autistic and neurotypical individuals and demonstrated a wide variety of imaging features exhibiting differences between groups. Our findings include several unreported feature measurements that demonstrate group-wise differences between autistic and neurotypical participants, including high volumetric variability of the corpus callosum in young ages, with average increases relative to the neurotypical group followed by an inversion of this effect to known decreases in corpus callosum volumes in later years. Autistic patients exhibited increased ETIV in the early years which account for the absolute increases observed in corpus callosum volume. We also observed white and gray matter volumes exhibiting a similar pattern (autistic increases early on followed by decreases in later years) in a variety of regions (see Table 1) that are potentially implicated in known symptoms of autism (see Table 2). We also demonstrated sustained increases in choroid plexus volumes among the autistic relative to the neurotypical participants.

Our findings could be indicative of autistic patients exhibiting an initial period of overgrowth, followed by a normalization that eventually results in autistic patients exhibiting volumetric reductions at later ages, in agreement with previous research (Courchesne et al., 2001, 2003), however, more research is needed to interpret these findings. Our findings include known increases in ventricular volumes among the autistic group, in agreement with the literature (Turner et al., 2016). However, we've extended those findings by showing that patients with autism also have, on average, larger volumes of the choroid plexuses.

The choroid plexuses are highly vascularized structures composed of numerous vili that are branched, and deeply immersed in the ventricles. The endothelium of their capillary vessels is fenestrated, which speaks in favor of their role in filtration of substances between blood and cerebrospinal fluid (CSF). However, evidence from molecular biology indicates that the choroid plexuses also function as secretory glands. The membranes of their cuboidal epithelial cells is composed of pumps, aquaporines, cotransporters, antiporters, and ion channels (Brown et al., 2004). Recent work (Lun et al., 2015) showed that the choroid plexuses exhibit regional differences in gene expression during development. Thus, enlargement of the volume of the choroid plexuses in autistic patients shown in our study might be linked with changes in signaling gradients across the cerebro-ventricular system (Lun et al., 2015) which in turn might contribute to alteration of histogenic processes that occur during development. This hypothesis, as well as our results, is further supported by the recent work of (Chaddad et al., 2017), whose study demonstrated that autistic patients have abnormalities in the spatial distribution of choroid plexus signal intensities as assessed with texture analysis.

Furthermore, until recently it has been believed that the cerebrospinal fluid (CSF) is formed and secreted by an active metabolic process that occurs exclusively within the choroid plexuses of the ventricles. However, this classic hypothesis has been challenged as numerous experiments failed to demonstrate it (for an excellent review, see Oreskovic and Klarica, 2010). For example, choroid plexotomy (removal of the choroid plexus) does not result in diminishment of CSF volume (Milhorat, 1976), nor with alteration of chemical composition of CSF (Hammock and Milhorat, 1973). Thus, recently it has been suggested that CSF, composed almost 99% of water, is both produced and reabsorbed through capillary walls of the central nervous system tissue (Bulat, 1993). This is highly dependent on osmotic and hydrostatic gradients of CSF and surrounding tissue (Oreskovic and Klarica, 2010). The new theory, however, does not underestimate the relevance of the choroid plexus in CSF volume formation, especially in conditions (i.e. inflammation) that change or alter hydrostatic and osmotic forces in CSF or surrounding tissue (Karimy et al., 2017). In light of the previously mentioned, it is possible that inflammation and inflammatory cytokine production (Zimmerman et al., 2005), together with enlargement of the choroid plexuses and their secretory role (Lun et al., 2015), alters osmotic pressure of CSF and causes enlargement of ventricles in patients with autism. Our findings demonstrate a positive correlation between ventricle volumes and choroid plexus volumes in both autistic and neurotypical patients (see Fig. 3). However, a direct causal relationship between choroid plexus volumes and ventricular volumes remains to be confirmed.

We have performed a preliminary validation with the Autism Brain Imaging Data Exchange (ABIDE) public dataset (Di Martino et al.,

2014). Results confirm these leading volumetric measurements relative to our BCH data: posterior corpus callosum (BCH: d = −0.66, ABIDE: d = −0.52), central corpus callosum (BCH: d = −0.67, ABIDE: AUC = −0.39), mid posterior corpus callosum (BCH: d = −0.66, ABIDE: d = −0.26), mid anterior corpus callosum (BCH: d = −0.47, ABIDE: d = −0.59), third ventricle (BCH: d = 0.70, ABIDE: d = 0.48), the right choroid plexus (BCH: d = 0.57, ABIDE: d = 0.39), and the right lateral ventricle (BCH: d = 0.56, ABIDE: d = 0.35). This confirmed our findings in each of our leading measurements (late adolescence) exhibiting reduced separation between the neurotypical and autistic groups in the ABIDE dataset with the exception of the mid anterior corpus callosum which exhibits a larger effect size in ABIDE. Reduced separation in the ABIDE dataset relative to BCH data in many of our validated measurements may be caused by differences in distributions of autistic severity in each group with the routine clinical BCH data likely to exhibit increased proportions of unhealthy autistic children which may also be correlated with more severe manifestations of autism. In contrast, the ABIDE dataset's autistic population's intelligence quotients (IQ) are similar to their typically developing counterparts (Di Martino et al., 2014), implying the dataset might disproportionately represent patients with high functioning autism.

We found regions of the brain potentially associated with disorders of visual facial processing including the inferior temporal region (Haxby et al., 2000), the inferior parietal region, which is involved in the perception of emotions in facial stimuli (Radua et al., 2010), the superior temporal region, which has been claimed to be involved in the perception of where others are directing their gaze, and is thought to be important in determining where others' emotions are being directed (Campbell et al., 1990), the fusiform region, which has been observed to influence the amygdala's response to emotional faces (Stephanou et al., 2016) and activation therein has been observed in autistic patients viewing faces (Hadjikhani et al., 2004), the lingual region, which appears to provide input to the ventral face area (McCarthy et al., 1999), the precuneus, which is involved in visuo-spatial imagery (Cavanna and Trimble, 2006) and the inferior temporal region, which is involved in visual object recognition (Logothetis and Sheinberg, 1996).

Identified brain regions potentially associated with disorders of speech and language include the bilateral superior temporal region which contains the primary auditory cortex (Bigler et al., 2007), the supramarginal region, which may be associated with language function as lesions therein may cause receptive aphasia, the middle temporal region, which has been identified as a critical node in the brain's language network (Acheson and Hagoort, 2013), the pars opercularis, which plays an important role in speech and language production (Foundas et al., 1998), the planum polare, reported to be part of a cortical "language network" (Koelsch et al., 2002), the caudate, which has been reported to exhibit language-dependent neuronal adaption (Crinion et al., 2006) and finally, the lingual and fusiform regions, which have been shown to be involved in language tasks (Mechelli et al., 2000).

Measurements demonstrating group-wise differences were also found in brain regions potentially associated with movement and motor control disorders including: the precentral region, which is a known motor area (Yousry et al., 1997), the caudate, damage to which has been associated with motor deficits (Pickett et al., 1998), the bilateral supramarginal gyrus, which is involved in the perception of space and limb locations, the left lateral occipital region and the bilateral inferior temporal gyrus (Brodmann's areas 18, 19, 37), which are involved in visual object recognition (Logothetis and Sheinberg, 1996), the precentral white matter, which is linked with the primary motor cortex (Brodmann's area 4), the superior parietal region, which is thought to be involved with spatial orientation, the precuneus, which is involved in attention to motor targets (Cavanna and Trimble, 2006), and finally, the superior temporal region, which mediates spatial awareness and exploration (Karnath et al., 2001).

Regions potentially linked with empathy deficits and disorders of emotional processing include the bilateral orbitofrontal region, which forms the basis for an existing test for autism (Stone et al., 1998), the insula, which is involved in the processing of norm violations (Sanfey et al., 2003), emotional processing (Phan et al., 2002) and empathy (Singer, 2006), the superior frontal region, which has been shown to activate with empathic judgments (Farrow et al., 2001), the superior temporal and the bilateral inferior parietal regions, which are involved in the perception of emotions in facial stimuli (Radua et al., 2010), the caudate, for which voxel based morphometry has demonstrated correlations with empathy (Rankin et al., 2006), the anterior cingulate, which has been linked with empathy for others' pain (Gu et al., 2010), the bilateral supramarginal region, which is thought to be associated with empathy (Silani, 2013), and finally, the precuneus, which has been shown to activate when a patient decides whether to act out of empathy and forgiveness (Farrow et al., 2001).

The main strength of this research study is that it incorporates large sample sizes in terms of the number of exams and also includes a wide range of patient ages while assessing what can be clinically accomplished in autistic imaging with MRI. This retrospective analysis included a cohort of very young patients who received imaging prior to their diagnosis of autism, a population particularly challenging to include in a traditional prospective study design, which typically involves the recruitment of patients based on a pre-existing diagnosis. Our dataset includes many examinations of patients aged 0–2.5 years, providing data on early stages of autism's development that is insufficient in the scientific literature. By including all samples available, we provide a thorough analysis of a clinical population, which is ideal for the assessment and development of diagnostic tests that would be applied to autistic patients receiving routine clinical imaging. Future generations of diagnostic technologies will be responsible for the correct identification of a variety of pathological conditions (such as autism) from large pools of patients assessed with routine clinical imaging.

Data acquisition with MRI involves measurement noise. Additional noise is introduced by FreeSurfer processing of MRI exams. Furthermore, there is a natural amount of variability in both the neurotypical population investigated, as well as in any autistic population. These factors result in substantial measurement variability when employing MRI and FreeSurfer to assess autistic and neurotypical participants. This variability may explain inconsistencies reported in the many MRI-based autism FreeSurfer studies that have been published in the literature, which are based on relatively small sample sizes, from widely ranging age groups, none of which cover the entire age range from newborn to adult (Groen et al., 2010; Jiao et al., 2010; Schumann et al., 2010; Schaer et al., 2013, 2015; Wallace et al., 2013; Ecker et al., 2014; Zielinski et al., 2014; Richter et al., 2015; Yang et al., 2016). With few samples available, differences between neurotypical and autistic groups may appear to exist when the observed effect could merely be a by-product of high levels of measurement variability. With high measurement variability, few samples and many measurements evaluated, some measurements will exhibit substantial group-wise differences by random chance. Insufficient sample sizes in the presence of high levels of measurement variability can result in erroneous findings. Measurement variability can also obscure real effects as non-statistically significant when sample sizes are low.

Our dataset includes many examinations of patients aged 0–2.5 years, providing data on early stages of autism's development that is minimal in the literature. By including all samples available, we provide a thorough analysis of a clinical population, which is ideal for the assessment and development of diagnostic tests that ultimately would be applied to autistic patients who are referred to routine clinical imaging. Future generations of diagnostic technologies will be responsible for the correct identification of a variety of pathological conditions (autism included) from large pools of patients assessed with routine clinical imaging, making clinically imaged autistic patients an interesting population for further research despite this group not having been studied in-depth.

A major limitation of this study is a lack of gold standard diagnoses for autism (ADI-R and ADOS evaluations were not available). This problem is caused by the retrospective nature of this study, for which it was not feasible to interview each patient and thus electronic patient medical records had to be relied upon. While indications of autism are typically entered into the electronic patient medical records by a Boston Children's Hospital physician, this does not guarantee that our dataset does not include patients whose autistic status was established by a community physician (ie. not an expert in diagnosing autism). Additionally, intelligence quotient (IQ) data was unavailable for the patients in this study. The retrospective nature of this study makes it impossible to account for all variables tracked and controlled for in prospective studies which include detailed patient interviews, but it is hoped that this work will identify anatomic and physiological effects of interest that will be thoroughly validated in carefully controlled future prospective studies. It is also hoped that this research can help bridge the gap between prospective studies and what can be achieved clinically. An additional limitation of our study was the need to include patients that are inferred to be neurotypical from routine clinical imaging. This was accomplished by excluding patients with indications of a long list of neurological issues while requiring each patient's MRI examination to have been assessed as normal by a neuroradiologist at BCH (Levman et al., 2017). This process yielded 993 examinations from patients deemed most likely to represent neurotypical individuals from a large pool of MRI examinations, in order to best approximate a typically developing population from a large-scale routine clinical imaging cohort. It is expected that the rate of false negatives (seemingly neurotypical patients who actually have a neurological issue) might be higher than the rate exhibited in typical well-controlled prospective studies and so may add variability to our neurotypical measurements and may represent an additional source of error in our study.

An additional limitation of this study is that it was performed retrospectively on patients that received an MRI for a wide variety of reasons. Among the patients in the neurotypical group, the leading reasons for the MRI examinations were headaches (60%), to rule out intracranial pathologies (13%), vomiting (11%) and night awakenings (10%). Among the autistic patients, the leading reasons for the MRI examinations were seizures (19%), to rule out intracranial pathologies (14%) and an abnormal EEG (9%). Since the population was drawn from routine clinical imaging, there is also a wide variety of comorbidities indicated in our patient's electronic medical records. The most common comorbidities in our neurotypical population are migraines (23%), headaches (19%) and abdominal pain (11%). The most common comorbidities in our autistic population are global developmental delay (26%), attention deficit hyperactivity disorder (16%), abdominal pain (14%) and epilepsy (13%). This study design was intended to provide a thorough analysis of a complete clinical population, providing a baseline of what to expect from other clinical populations and facilitating research into novel diagnostic tests which would be applied to populations akin to the one investigated in this study. Traditional prospective MRI studies often involve imaging patients who are much healthier than is realistic clinically. The study design presented here allows for the assessment of what can be accomplished in the context of large-scale clinical imaging.

There is variability in imaging parameters (spatial resolution, signal-to-noise ratio etc.) caused by variations in the pulse sequences employed; however, imaging was performed with a suite of 3 T Siemens MRI scanners all installed at BCH in 2007. Ideally, this study would be performed on scans using a single MRI protocol; however, doing so would greatly reduce the number of samples available for inclusion. Large sample sizes help overcome potential bias associated with measurements that exhibit considerable variability. While limiting the analysis to a single imaging protocol would reduce potential bias caused by scan parameter variability, it would increase bias induced by sample size effects. Many measurements produced by FreeSurfer on our BCH dataset demonstrate that the discriminating power (between autistic and neurotypical patients) of volumetric measurements (in mm^3) is approximately identical to the discriminating power of the voxel count measurements in those same regions (this includes ventricular volumes/voxel counts and corpus callosum volumes/voxel counts). Since voxel counts vary greatly with spatial resolution variations, we believe the effect on our results caused by varying spatial resolutions in our MR protocols to be modest.

An additional limitation of this study is that the age distributions of available patients for the two groups vary considerably (Fig. 1), because of the availability of patients that met our inclusion criteria from a large clinical population. This inevitably resulted in imbalanced patient populations for further analysis. Our experiment did not involve age- or gender-based patient matching between our groups. Instead, we have opted to perform our statistical analyses in a group-wise manner, varying the age range under consideration, and to plot our main findings on an age-dependent basis while differentiating between female and male patients in our scatter plots (Fig. 2). This methodology was selected to avoid the reduced sample size that would arise from only including those autistic patients who have a neurotypical counterpart with identical age and the same gender. Additionally, this methodology was selected to avoid having our analysis be influenced by the extent of difference between matched pairs of individuals, for which a variety of factors beyond age and gender might influence how appropriate it is for the patients to have been paired (brain volume, sub-structure volume, co-morbidities, etc.). We also performed a multivariate regression analysis that controls for the effects of age, gender, intracranial volume and several comorbidities to confirm that these factors are not the cause of our reported findings.

An additional limitation of this study is that FreeSurfer is not optimized for the youngest patients in our population. As such, the rate at which FreeSurfer fails to extract measurements from clinical MRI examinations increases substantially for participants aged 0–8 months-old and the reliability of the results successfully produced by FreeSurfer on patients from this age range is uncertain. This issue likely contributes to increased measurement variability in the early years in our experiment. FreeSurfer's reliability was assessed as reasonable for patients 8-months-old and later (considering this is beyond the validated age range for the technology), at which point myelination contrast patterns have inverted so as to match the general pattern exhibited through the rest of life (with gray contrast located on the brain's periphery and white contrast occupying central regions). It was noted that, in particular, frontal regions had a tendency to be undersegmented. Research aimed at overcoming the problem of FreeSurfer's applicability and reliability in very young populations (de Macedo Rodrigues et al., 2015; Zollei et al., 2017) will be incorporated into future work, which will also involve the extension of this analysis to tractography and functional MRI (fMRI) as well as to perform a detailed and thorough validation with the ABIDE dataset.

Additional future work will involve correlating our dataset with detailed clinical information not available in our electronic patient medical records. This large-scale task may allow us to assess the potential association between MRI measurements and symptom severity, outcomes etc. Future work will also look at comparing the autistic group with groups at high risk for autism and groups that present similarly to autism in order to extend this work's diagnostic assessments to differential diagnosis.

Our results indicate that automatically extracted measurements can be used to predict the pathological status of a patient whose brain has been imaged with MRI; however, future work is needed to optimize the performance of such diagnostic testing. Future work will look at improving our ability to discriminate between autistic and neurotypical patients with the help of additional MRI modalities, such as tractography and fMRI as well as with multivariate analysis. It is hoped that these research avenues will assist toward better understanding autism as well as assisting with improved characterization, diagnosis and classification of the disorder into subtypes.

Acknowledgments

The authors would like to thank Dr. Henry Feldman, PrincipalBiostatistician at Boston Children's Hospital for advice on conducting statistical analyses. This work was supported by the National Institutes of Health (grant numbers R01HD078561, R03NS091587) to ET; Natural Science and Engineering Research Council of Canada's Canada Research Chair grant (grant number 231266) to JL, a Canada Foundation for Innovation and Nova Scotia Research and Innovation Trust infrastructure grant (R0176004) to JL and a St. Francis Xavier University research startup grant to JL (grant number R0168020).

References

Acheson, D.J., Hagoort, P., 2013. Stimulating the brain's language network: syntactic ambiguity resolution after TMS to the inferior frontal gyrus and middle temporal gyrus. J. Cogn. Neurosci. 25 (10), 1664–1677.
Amaral, D.G., Schumann, C.M., Nordahl, C.W., 2008. Neuroanatomy of autism. Trends Neurosci. 31 (3), 137–145.
Behrmann, M., Thomas, C., Humphreys, K., 2006. Seeing it differently: visual processing in autism. Trends Cogn. Sci. 10 (6), 258–264.
Bigler, E.D., Mortensen, S., Neeley, E.S., Ozonoff, S., Krasny, L., Johnson, M., Lu, J., Provencal, S.L., McMahon, W., Lainhart, J.E., 2007. Superior temporal gyrus, language function, and autism. Dev. Neuropsychol. 31 (2), 217–238.
Brown, P., Davies, S., Speake, T., Millar, I., 2004. Molecular mechanisms of cerebrospinal fluid production. Neuroscience 129, 955–968.
Bulat, M., 1993. Dynamics and statics of the cerebrospinal fluid: the classical and a new hypothesis. Intracranial Pressure VIII. Springer, pp. 726–730.
Bunge, S.A., Dudukovic, N.M., Thomason, M.E., Vaidya, C.J., Gabrieli, J.D., 2002. Immature frontal lobe contributions to cognitive control in children: evidence from fMRI. Neuron 33 (2), 301–311.
Campbell, R., Heywood, C.A., Cowey, A., Regard, M., Landis, T., 1990. Sensitivity to eye gaze in prosopagnosic patients and monkeys with superior temporal sulcus ablation. Neuropsychologia 28 (11), 1123–1142.
Casey, B.J., Trainor, R.J., Orendi, J.L., Schubert, A.B., Nystrom, L.E., Giedd, J.N., Castellanos, F.X., Haxby, J.V., Noll, D.C., Cohen, J.D., Forman, S.D., Dahl, R.E., Rapoport, J.L., 1997. A developmental functional MRI study of prefrontal activation during performance of a go-no-go task. J. Cogn. Neurosci. 9 (6), 835–847.
Cavanna, A.E., Trimble, M.R., 2006. The precuneus: a review of its functional anatomy and behavioral correlates. Brain 129 (3), 564–583.
Chaddad, A., Desrosiers, C., Toews, M., 2017. Multi-scale radiomic analysis of sub-cortical regions in MRI related to autism, gender and age. Sci. Rep. 7, 45639.
Courchesne, E., Karns, C.M., Davis, H.R., Ziccardi, R., Carper, R.A., Tigue, Z.D., Chisum, H.J., Moses, P., Pierce, K., Lord, C., Lincoln, A.J., Pizzo, S., Schreibman, L., Haas, R.H., Akshoomoff, N.A., Courchesne, R.Y., 2001. Unusual brain growth patterns in early life in patients with autistic disorder. Neurology 57 (2), 245–254.
Courchesne, E., Carper, R., Akshoomoff, N., 2003. Evidence of brain overgrowth in the first year of life in autism. JAMA 290, 337–344.
Crinion, J., Turner, R., Grogan, A., Hanakawa, T., Noppeney, U., Devlin, J.T., Aso, T., Urayama, S., Fukuyama, H., Stockton, K., Usui, K., Green, D.W., Price, C.J., 2006. Language control in the bilateral brain. Science 312 (5779), 1537–1540.
de Macedo Rodrigues, K., Ben-Avi, E., Sliva, D.D., Choe, M., Drottar, M., Wang, R., Fischl, B., Grant, P.E., Zollei, L., 2015. A FreeSurfer-compliant consistent manual segmentation of infant brains spanning the 0–2 year age range. Front. Hum. Neurosci. 9, 21.
Di Martino, A., Yan, C.-G., Li, Q., Denio, E., Castellanos, F.X., Alaerts, K., Anderson, J.S., et al., 2014. The Autism Brain Imaging Data Exchange: towards large-scale evaluation of the intrinsic brain architecture in autism. Mol. Psychiatry 19 (6), 659–667.
Dziobek, I., Bahnemann, M., Convit, A., Heekeren, H.R., 2010. The role of the fusiform-amygdala system in the pathophysiology of autism. Arch. Gen. Psychiatry 67 (4), 397–405.
Dziuk, M.A., Gidley Larson, J.C., Apostu, A., Mahone, E.M., Denckla, M.B., Mostofsky, S.H., 2007. Dyspraxia in autism: association with motor, social, and communicative deficits. Dev. Med. Child Neurol. 49 (10), 734–739.
Ecker, C., Marquand, A., Mourao-Miranda, J., Johnston, P., Daly, E.M., Brammer, M.J., Maltezos, S., Murphy, C.M., Robertson, D., Williams, S.C., Murphy, D.G., 2010. Describing the brain in autism in five dimensions—magnetic resonance imaging-assisted diagnosis of autism spectrum disorders using a multiparameter classification approach. J. Neurosci. 30 (32), 10612–10623.
Ecker, C., Ginestet, C., Feng, Y., Johnston, P., Lombardo, M.V., Lai, M.C., Suckling, J., Palaniyappan, L., Daly, E., Murphy, C.M., Williams, S.C., Bullmore, E.T., Baron-Cohen, S., Brammer, M., Murphy, D.G., AIMS Consortium, M.R.C., 2013. Brain surface anatomy in adults with autism the relationship between surface area, cortical thickness, and autistic symptoms. JAMA Psychiatry 70 (1), 59–70.
Ecker, C., Shahidiani, A., Feng, Y., Daly, E., Murphy, C., D'Almeida, V., Deoni, S., Williams, S.C., Gillan, N., Gudbrandsen, M., Wichers, R., Andrews, D., Van Hemert, L., Murphy, D.G., 2014. The effect of age, diagnosis, and their interaction on vertex-based measures of cortical thickness and surface area in autism spectrum disorder. J. Neural Transm. 121 (9), 1157–1170.
Fair, D.A., Cohen, A.L., Power, J.D., Dosenbach, N.U., Church, J.A., Miezin, F.M., Schlaggar, B.L., Petersen, S.E., 2009. Functional brain networks develop from a "local to distributed" organization. PLoS Comput. Biol. 5 (5), e1000381.
Farrow, T.F.D., Zheng, Y., Wilkinson, I.D., Spence, S.A., Deakin, J.F.W., Tarrier, N., Griffiths, P.D., Woodruff, P.W.R., 2001. Investigating the functional anatomy of empathy and forgiveness. NeuroReport 12 (11), 2433–2438.
Fischl, B., 2012. FreeSurfer. NeuroImage 62 (2), 774–781.
Foundas, A.L., Eure, K.F., Luevano, L.F., Weinberger, D.R., 1998. MRI asymmetries of Broca's area: the pars triangularis and pars opercularis. Brain Lang. 64 (3), 282–296.
Fox, M.D., Snyder, A.Z., Vincent, J.L., Corbetta, M., Van Essen, D.C., Raichle, M.E., 2005. The human brain is intrinsically organized into dynamic, anticorrelated functional networks. Proc. Natl. Acad. Sci. U. S. A. 102, 9673–9678.
Gillberg, C., 1993. Autism and related behaviours. J. Intellect. Disabil. Res. 37 (Pt. 4), 343–372.
Gogtay, N., Giedd, J.N., Lusk, L., Hayashi, K.M., Greenstein, D., Vaituzis, A.C., Nugent 3rd, T.F., Herman, D.H., Clasen, L.S., Toga, A.W., Rapoport, J.L., Thompson, P.M., 2004. Dynamic mapping of human cortical development during childhood through early adulthood. Proc. Natl. Acad. Sci. U. S. A. 101 (21), 8174–8179.
Groen, W., Teluij, M., Buitelaar, J., Tendolkar, I., 2010. Amygdala and hippocampus enlargement during adolescence in autism. J. Am. Acad. Child Adolesc. Psychiatry 49 (6), 552–560.
Gu, X., Liu, X., Guise, K.G., Naidich, T.P., Hof, P.R., Fan, J., 2010. Functional dissociation of the frontoinsular and anterior cingulate cortices in empathy for pain. J. Neurosci. 30 (10), 3739–3744.
Haar, S., Berman, S., Behrmann, M., Dinstein, I., 2016. Anatomical Abnormalities in Autism? Cereb. Cortex 26 (4), 1440–1452.
Hadjikhani, N., Joseph, R.M., Snyder, J., Chabris, C.F., Clark, J., Steele, S., McGrath, L., Vangel, M., Aharon, I., Feczko, E., Harris, G.J., Tager-Flusberg, H., 2004. Activation of the fusiform gyrus when individuals with autism spectrum disorder view faces. NeuroImage 22, 1140–1150.
Hammock, M.K., Milhorat, T.H., 1973. Recent studies on the formation of cerebrospinal fluid. Dev. Med. Child Neurol. 15, 27–34.
Haxby, J.V., Hoffman, E.A., Gobbini, M.I., 2000. The distributed human neural system for face perception. Trends Cogn. Sci. 4 (6), 223–233.
Jiao, Y., Chen, R., Ke, X., Chu, K., Lu, Z., Herskovits, E.H., 2010. Predictive models of autism spectrum disorder based on brain regional cortical thickness. NeuroImage 50 (2), 589–599.
Jones, A.P., Happe, F.G., Gilbert, F., Burnett, S., Viding, E., 2010. Feeling, caring, knowing: different types of empathy deficit in boys with psychopathic tendencies and autism spectrum disorder. J. Child Psychol. Psychiatry 51 (11), 1188–1197.
Karimy, J.K., Zhang, J., Kurland, D.B., Theriault, B.C., Duran, D., Stokum, J.A., Furey, C.G., Zhou, X., Mansuri, M.S., Montejo, J., 2017. Inflammation-dependent cerebrospinal fluid hypersecretion by the choroid plexus epithelium in posthemorrhagic hydrocephalus. Nat. Med. 23, 997.
Karnath, H.O., Ferber, S., Himmelbach, M., 2001. Spatial awareness is a function of the temporal not the posterior parietal lobe. Science 411 (6840), 950–953.
Kellerman, G., Fan, J., Gorman, J.M., 2005. Auditory abnormalities in autism: toward functional distinctions among findings. CNS Spectr. 10, 748–756.
Koelsch, S., Gunter, T.C., Cramon, D.Y., Zysset, S., Lohmann, G., Friederici, A.D., 2002. Bach speaks: a cortical "Language-Network" serves the processing of music. NeuroImage 17 (2), 956–966.
Lefebvre, A., Beggiato, A., Bourgeron, T., Toro, R., 2015. Neuroanatomical diversity of corpus callosum and brain volume in autism: meta-analysis, analysis of the autism brain imaging data exchange project, and simulation. Biol. Psychiatry 78 (2), 126–134.
Levman, J., MacDonald, P., Lim, A.R., Forgeron, C., Takahashi, E., 2017. A Pediatric Structural MRI Analysis of Healthy Brain Development From Newborns to Young Adults. Published Online Ahead of Print Edition at Human Brain Mapping, pp. 12 September 12th, 2017.
Logothetis, N.K., Sheinberg, D.L., 1996. Visual object recognition. Annu. Rev. Neurosci. 19, 577–621.
Lun, M.P., Johnson, M.B., Broadbelt, K.G., Watanabe, M., Kang, Y.J., Chau, K.F., Springel, M.W., Malesz, A., Sousa, A.M., Pletikos, M., Adelita, T., Calicchio, M.L., Zhang, Y., Holtzman, M.J., Lidov, H.G., Sestan, N., Steen, H., Monuki, E.S., Lehtinen, M.K., 2015. Spatially heterogeneous choroid plexus transcriptomes encode positional identity and contribute to regional CSF production. J. Neurosci. 35, 4903–4916.
McCarthy, G., Puce, A., Belger, A., Allison, T., 1999. Electrophysiological studies of human face perception. II: response properties of face-specific potentials generated in occipitotemporal cortex. Cereb. Cortex 9 (1), 431–444.
McIntosh, A.R., Bookstein, F.L., Haxby, J.V., Grady, C.L., 1996. Spatial pattern analysis of functional brain images using partial least squares. NeuroImage 3, 143–157.
Mechelli, A., Humphreys, G.W., Mayall, K., Olson, A., Price, C.J., 2000. Differential effects of word length and visual contrast in the fusiform and lingual gyri during reading. Proc. Biol. Sci. 267 (1455), 1909–1913.
Mesulam, M.M., 1981. A cortical network for directed attention and unilateral neglect. Ann. Neurol. 10, 309–325.
Milhorat, T.H., 1976. Structure and function of the choroid plexus and other sites of cerebrospinal fluid formation. Int. Rev. Cytol. 47, 225–288.
Oreskovic, D., Klarica, M., 2010. The formation of cerebrospinal fluid: nearly a hundred years of interpretations and misinterpretations. Brain Res. Rev. 64, 241–262.
Phan, K.L., Wager, T., Taylor, S.F., Liberzon, I., 2002. Functional neuroanatomy of emotion: a meta-analysis of emotion activation studies in PET and fMRI. NeuroImage 16 (2), 331–348.
Pickett, E.R., Kuniholm, E., Protopapas, A., Friedman, J., Lieberman, P., 1998. Selective speech motor, syntax, and cognitive deficits associated with bilateral damage to the putamen and the head of the caudate nucleus: a case study. Neuropsychologia 36 (2), 173–188.
Pienaar, R., Rannou, N., Haehn, D., Grant, P.E., 2014. ChRIS: real-time web-based MRI

data collection analysis, and sharing. 20th Annual Meeting of the Organization for Human Brain Mapping, vol. 5.
Radua, J., Phillips, M.L., Russel, T., Lawrence, N., Marshall, N., Kalidindi, S., El-Hage, W., McDonald, C., Giampietro, V., Brammer, M.J., David, A.S., Surguladze, S.A., 2010. Neural response to specific components of fearful faces in healthy and schizophrenic adults. NeuroImage 49 (1), 939–946.
Rankin, K.P., Gorno-Tempini, M.L., Allison, S.C., Stanley, C.M., Glenn, S., Weiner, M.W., Miller, B.L., 2006. Structural anatomy of empathy in neurodegenerative disease. Brain 129 (11), 2945–2956.
Reiss, A.L., Abrams, M.T., Singer, H.S., Ross, J.L., Denckla, M.B., 1996. Brain development, gender and IQ in children. A volumetric imaging study. Brain 119 (Pt. 5), 1763–1774.
Richter, J., Poustka, L., Vomstein, K., Haffner, J., Parzer, P., Stieltjes, B., Henze, R., 2015. Volumetric alterations in the heteromodal association cortex in children with autism spectrum disorder. Eur. Psychiatry 30 (2), 214–220.
Sanfey, A.G., Rilling, J.K., Aronson, J.A., Nystrom, L.E., Cohen, J.D., 2003. The neural basis of economic decision-making in the ultimatum game. Science 300 (5626), 1755–1758.
Schaer, M., Ottet, M.C., Scariati, E., Dukes, D., Franchini, M., Eliez, S., Glaser, B., 2013. Decreased frontal gyrification correlates with altered connectivity in children with autism. Front. Hum. Neurosci. 7, 750.
Schaer, M., Kochalka, J., Padmanabhan, A., Supekar, K., Menon, V., 2015. Sex differences in cortical volume and gyrification in autism. Mol. Autism 6, 42.
Schumann, C.M., Bloss, C.S., Carter Barnes, C., Wideman, G.M., Carper, R.A., Akshoomoff, N., Pierce, K., Hagler, D., Schork, N., Lord, C., Courchesne, E., 2010. Longitudinal magnetic resonance imaging study of cortical development through early childhood in autism. J. Neurosci. 30 (12), 4419–4427.
Silani, C., 2013. I'm OK, you're not OK: right supramarginal gyrus plays an important role in empathy. ScienceDaily 9 (October).
Singer, T., 2006. The neuronal basis and ontogeny of empathy and mind reading: review of literature and implications for future research. Neurosci. Biobehav. Rev. 30 (6), 855–863.
Stephanou, K., Davey, C.G., Kerestes, R., Whittle, S., Pujol, J., Yucel, M., Fornito, A., Lopez-Sola, M., Harrison, B.J., 2016. Brain functional correlates of emotion regulation across adolescence and young adulthood. Hum. Brain Mapp. 37 (1), 7–19.
Stone, V.E., Baron-Cohen, S., Knight, R.T., 1998. Frontal lobe contributions to theory of mind. J. Med. Investig. 10, 640–656.
Student, S., 1908. The probable error of a mean. Biometrika. 6 (1), 1–25.
Supekar, K., Musen, M., Menon, V., 2009. Development of large-scale functional brain networks in children. PLoS Biol. 7 (7), e1000157.
Thomas, K.M., Drevets, W.C., Whalen, P.J., Eccard, C.H., Dahl, R.E., Ryan, N.D., Casey, B.J., 2001. Amygdala response to facial expressions in children and adults. Biol. Psychiatry 49 (4), 309–316.
Toal, F., Murphy, D.G., Murphy, K.C., 2005. Autistic-spectrum disorders: lessons from neuroimaging. Br. J. Psychiatry 187, 395–397.
Turner, A.H., Greenspan, K.S., van Erp, T.G.M., 2016. Pallidum and lateral ventricle volume enlargement in autism spectrum disorder. Psychiatry Res. 252, 40–45.
Vaadia, E., Haalman, I., Abeles, M., Bergman, H., Prut, Y., Slovin, H., Aertsen, A., 1995. Dynamics of neuronal interactions in monkey cortex in relation to behavioural events. Nature 373, 515–518.
Wallace, G.L., Robustelli, B., Dankner, N., Kenworthy, L., Giedd, J.N., Martin, A., 2013. Increased gyrification, but comparable surface area in adolescents with autism spectrum disorders. Brain 136 (Pt 6), 1956–1967.
Wan, C.Y., Schlaug, G., 2010. Neural pathways for language in autism: the potential for music-based treatments. Future Neurol. 5 (6), 797–805.
Wing, L., 1997. The autistic spectrum. Lancet 350 (9093), 1761–1766.
Yang, D., Beam, D., Pelphrey, K.A., Abdullahi, S., Jou, R.J., 2016. Cortical morphological markers in children with autism: a structural magnetic resonance imaging study of thickness, area, volume, and gyrification. Mol. Autism 7, 11.
Youngstrom, E.A., 2014. A primer on receiver operating characteristic analysis and diagnostic efficiency statistics for pediatric psychology: we are ready to ROC. J. Pediatr. Psychol. 39 (2), 204–221.
Yousry, T.A., Schmid, U.D., Alkadhi, H., Schmidt, D., Peraud, A., Buettner, A., Winkler, P., 1997. Localization of the motor hand area to a knob on the precentral gyrus. A new landmark. Brain 120 (1), 141–157.
Zielinski, B.A., Prigge, M.B., Nielsen, J.A., Froelich, A.L., Abildskov, T.J., Anderson, J.S., Fletcher, P.T., Zygmunt, K.M., Travers, B.G., Lange, N., Alexander, A.L., Bigler, E.D., Lainhart, J.E., 2014. Longitudinal changes in cortical thickness in autism and typical development. Brain 137 (Pt. 6), 1799–1812.
Zimmerman, A.W., Jyonouchi, H., Comi, A.M., Connors, S.L., Milstien, S., Varsou, A., Heyes, M.P., 2005. Cerebrospinal fluid and serum markers of inflammation in autism. Pediatr. Neurol. 33, 195–201.
Zollei, L., Ou, Y., Iglesias, J., Grant, P.E., Fischl, B., 2017. FreeSurfer image processing pipeline for infant clinical MRI images. Proceedings of the Organization for Human Brain Mapping Conference, vol. 1703.